Scripta Materialia 145 (2018) 71–75

Contents lists available at ScienceDirect

Scripta Materialia

journal homepage: www.elsevier.com/locate/scriptamat

Regular article

Stability of vacancy-type defect clusters in Ni based on first-principles and molecular dynamics simulations☆

Shijun Zhao [a,*], Yanwen Zhang [a,b,*], William J. Weber [b,a]

[a] Materials Science and Technology Division, Oak Ridge National Laboratory, Oak Ridge, TN 37831, USA
[b] Department of Materials Science and Engineering, University of Tennessee, Knoxville, TN 37996, USA

ARTICLE INFO

Article history:
Received 29 August 2017
Received in revised form 3 October 2017
Accepted 4 October 2017
Available online xxxx

Keywords:
Vacancy clusters
Stacking fault tetrahedra
First-principles calculations
Ab initio molecular dynamics

ABSTRACT

Using first-principles calculations based on density-functional theory, the energetics of different vacancy-type defects, including voids, stacking fault tetrahedra (SFT) and vacancy loops, in Ni are investigated. It is found that voids are more stable than SFT at 0 K, which is also the case after taking into account the volumetric strains. By carrying out *ab initio* molecular dynamics simulations at temperatures up to 1000 K, direct transformations from vacancy loops and voids into SFT are observed. Our results suggest the importance of temperature effects in determining thermodynamic stability of vacancy clusters in face-centered cubic metals.

In face-centered cubic (*fcc*) metals, agglomeration of vacancies usually leads to the formation of voids, vacancy-type dislocation loops and stacking fault tetrahedra (SFT). It is generally regarded that SFT are the dominant type of vacancy clusters in low stacking fault energy (SFE) materials, such as Ni [1–3]. Different formation mechanisms of SFT have been proposed previously, including dissociation of [111] Frank vacancy loops [4], collapse of vacancy clusters [5], aggregation of vacancies [6], and directly within collision cascades [7]. However, these proposed mechanisms are mostly inferred from molecular dynamics simulations whose fidelity relies on the reliability of empirical interatomic potentials. Another concern is that different potentials yield distinct, but often different, conclusions as to the equilibrium structures of vacancy clusters. A typical example is the stable form of vacancy clusters predicted by different embedded atom method (EAM) potentials. While the Bonny2013 potential [8] predicts SFT are the most stable forms of vacancy type defects in Ni, the Bonny2011 potential [9] suggests that [111] Frank vacancy loops are more preferred [10]. The potential-dependent properties of vacancy clusters are also found in a previous study for Cu [11]. These observations point to the need for accurate calculations, independent of any specific potential models. As a cross-check, first-principles calculations can be employed to study the stability of different vacancy-type defects and provide accurate results compared to those from empirical potentials. Nevertheless, this approach is restricted by the system size required for the study of vacancy clusters.

Experimentally, the properties of vacancy clusters in materials are of great interest for material performance in a radiation environment, since the formation and growth of vacancy clusters may lead to significant volumetric swelling [12]. For Ni, both SFT and vacancy loops are observed after ion irradiation at room temperature. For example, it is reported that the majority (90%) of vacancy clusters are SFT in Ar irradiated Ni [13]. However, other studies show that the majority of vacancy clusters (61.8%) are in the form of loops in Kr^+ irradiated Ni [14]. Besides SFT and vacancy loops, the clustering of vacancies can lead to the creation of voids (three-dimensional empty spaces in the crystal structure), which is also an important vacancy-type defect.

In this work, the energetics of various vacancy clusters in Ni is investigated using *ab initio* calculations in relatively large supercells. The configurations considered are SFT, voids and vacancy platelets of hexagonal and triangular shapes on the [111] plane. Our calculations indicate that voids are more stable than the corresponding SFT configurations with the same number of vacancies. This relative stability is not influenced even by taking into account of volumetric strain (lattice expansion or compression). Through *ab initio* molecular dynamics (AIMD) simulations, direct transformations of voids or vacancy loops to SFT are observed, suggesting that SFT are more stable thermodynamically.

* Corresponding authors.
E-mail addresses: zhaos@ornl.gov (S. Zhao), zhangy1@ornl.gov (Y. Zhang).

https://doi.org/10.1016/j.scriptamat.2017.10.003
1359-6462/

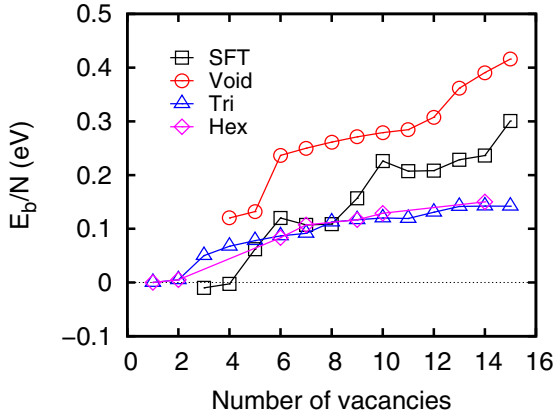

Fig. 1. Binding energies per vacancy for different vacancy clusters in pure Ni: SFT, voids and vacancy platelets of triangular (Tri) and hexagonal (Hex) shapes on the [111] plane.

Ab initio calculations were carried out based on density-functional theory as implemented in the Vienna *ab initio* simulation package (VASP) [15]. A gradient corrected functional in the Perdew-Burke-Ernzerhof (PBE) form was used to describe the exchange and correlation interactions [16]. Electron-ion interactions were treated within the projector-augmented-wave (PAW) method [17]. The energy cutoff for the plane-wave basis set was set to be 270 eV. All calculations were performed with spin-polarization to account for magnetic properties. For structural optimizations, the energy convergence was set to be 10^{-4} eV and the atomic positions were relaxed by minimizing the Hellmann-Feynman forces on each atom to less than 10^{-2} eV/Å. Periodic boundary conditions were employed. The calculation of defect clusters requires large supercells to reduce the interactions among the defects and their periodic images. In this work, a $5 \times 5 \times 5$ supercell containing 500 atoms was used, and the energetics of vacancy clusters with 1 to 15 vacancies were studied. Owing to the large supercell, only Γ point was included in the calculations. The formation energy, E_f^{Nv}, of a vacancy cluster with N vacancies in a N_p-atom perfect supercell was calculated by $E_f^{Nv} = E - E_0 + \frac{N}{N_p} E_0$, where E and E_0 are the total energy of defective and perfect supercells, respectively. The binding energy, E_b^N, was then obtained by $E_b = NE_f^v - E_f^{Nv}$.

The used energy cutoff and kpoint are first tested to ensure the convergence regarding the reported energetics of vacancies. The calculated formation energy of a single vacancy in a 500-atoms supercell is 1.47 eV with our calculation parameters, in good agreement with a previous result of 1.47 eV [18]. Increasing energy cutoff to 400 eV leads to 1.48 eV, while increasing kpoint to $2 \times 2 \times 2$ also results in 1.48 eV. For vacancy clusters, a difference of 0.03 eV in calculated binding energy of a 15*v*-SFT is observed when increasing to $2 \times 2 \times 2$ kpoints. The results suggest that our calculations are reliable to give accurate energetics for vacancies in Ni. Previous studies suggest that the PBE functional is better to describe the properties of Ni [19]. This functional form is, therefore, used in this study.

Four different types of vacancy clusters are considered, namely, triangular loops, hexagonal loops, SFT and voids. When vacancy number N is a magic number, the structure of corresponding vacancy cluster is definitive. However, those non-magic vacancy number clusters may take many different shapes. In this case, several competitive structures are studied and only those structures with the lowest energy are reported. The methodology to construct different vacancy clusters is given as follows. For [111] triangular vacancy loops, their structures from 1*v*–3*v* are unambiguous. For 4*v*, there are two configurations, in which the difference resides in the location of the fourth vacancy. Our calculations show that a rhombus-shaped structure is more energetically favorable. Therefore, we take this rule as a principle to construct other imperfect vacancy loops by adding additional vacancies starting from the edge center outside the magic number vacancy loops. Similar methodology is used to construct hexagonal vacancy loops. In this case, $N = 7$ corresponds to a perfect hexagonal vacancy loop. Larger loops are created by placing additional vacancies at the edge center. Imperfect SFT structures are constructed with the help of classical molecular dynamics (LAMMPS code [20]) based on the Mishin potential [21]. By taking the constructed vacancy loop as input, a short MD simulation at 600 K was carried out followed by an energy minimization. The obtained structure is then fed into *ab initio* calculations to further calculate the energy. We have compared energies of different SFT structures obtained from different initial loop configurations as described above and reported the lowest energy ones. To construct void structures with n vacancies, we delete an atom in the center together with its $(n - 1)$ nearest neighbors, as did in a previous study [5]. However, other configurations in tetrahedral and octahedral shapes are also considered. It should be pointed out that, in the calculation process, we also made a literature survey on vacancy clusters in *fcc* metals to cross-check our results [22,23]. A complete list of stable configurations identified in our calculations is provided in Supplementary materials. The calculated binding energies of different vacancy clusters considered are provided in Fig. 1.

The results in Fig. 1 indicate that [111] vacancy loops in either triangular or hexagonal shape have similar binding energies. The binding energies of the corresponding SFT are higher than those of vacancy loops when the vacancy number is larger than 6. Besides, there are local maximums in the binding energies of SFT, such as 6, 10 and 15, suggesting that these perfect SFT are rather stable. Surprisingly, it is observed that the binding energies of voids are always larger than those of SFT containing the same number of vacancies, despite the fact that vacancy clusters in Ni are often found in the form of SFT instead of voids in experiments [24]. This discrepancy does not necessarily indicate the failure of DFT, since these energies are calculated at 0 K without consideration of thermal effects. Note that energy differences between

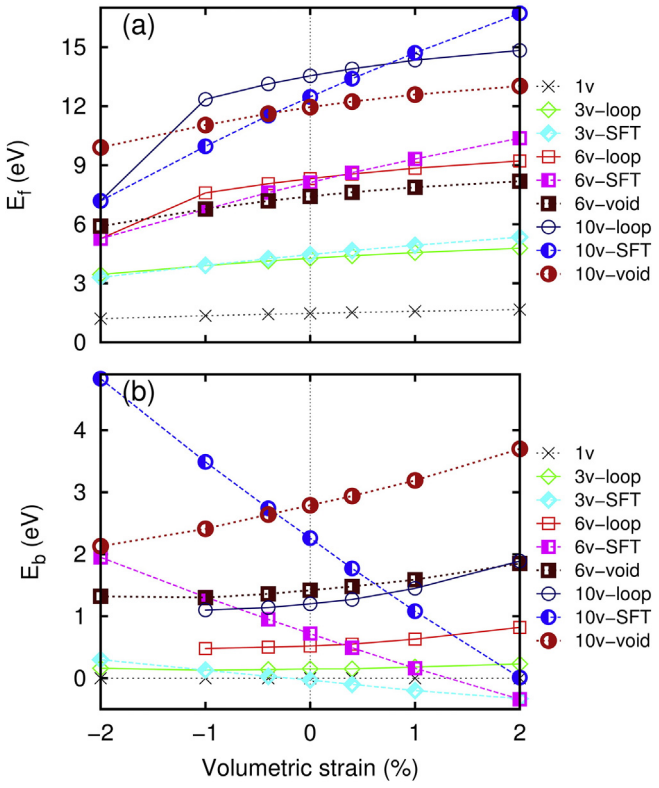

Fig. 2. Formation and binding energies of different vacancy clusters as a function of volumetric strain. Because of the similar binding energies between triangular and hexagonal vacancy loops, only the triangular vacancy loops are considered.

voids and SFT do not decrease with increasing vacancy numbers, suggesting their relative stabilities are not changed even for larger clusters.

The ground state calculations show that the stable divacancy in Ni (consists of two vacant sites at two nearest-neighbor sites) has a binding energy of 0.01 eV, an indication of the weak binding between them. The weakness of the divacancy binding suggests that the aggregation of vacancies is unlikely. For three vacancies, the binding energy of the [111] loop (3*v*-loop) is 0.05 eV per vacancy, while it is only −0.01 eV per vacancy for the stacking fault tetrahedron configuration (3*v*-SFT). This result suggests that the interactions among vacancies are repulsive in this case because of the negative binding energy. In this configuration, an atom in the nearby [111] plane is displaced towards the 3*v*-loop, creating a Frenkel pair. For $N_v = 4$, a tetrahedron vacancy configuration in which four vacancies as vertices exhibit the highest binding energy compared to SFT and loop configurations. For $N_v = 6$ and 10, perfect SFT structures are obtained, but their binding energies are lower than the corresponding void-like structures. Here, an octahedral void at $N_v = 6$ and a tetrahedron void at $N_v = 10$ are more stable.

To further evaluate the stability of different vacancy clusters, the effect of volumetric strain is considered by increasing or decreasing the lattice constant isotopically. The strain is defined as $\varepsilon = (a - a_0) / a_0$, where a and a_0 are the modified and pristine lattice constant of Ni, respectively. The calculated formation and binding energies of different vacancy clusters as a function of both tension and compression strains are provided in Fig. 2. It shows that the formation energy of a single vacancy in Ni increases continuously with increasing tension strain and decreases with increasing compression strain, in accordance with previous results [25]. Note that the highest tensile strain of 2% considered in the present study corresponds to the thermal expansion coefficient at 1429 K for pure Ni [26]. For all other vacancy clusters considered, the variation of their formation energies follows the same trend as that of a single vacancy. Another notable feature is that the 6*v*-loop and 10*v*-loop spontaneously transform to SFT configurations after structural

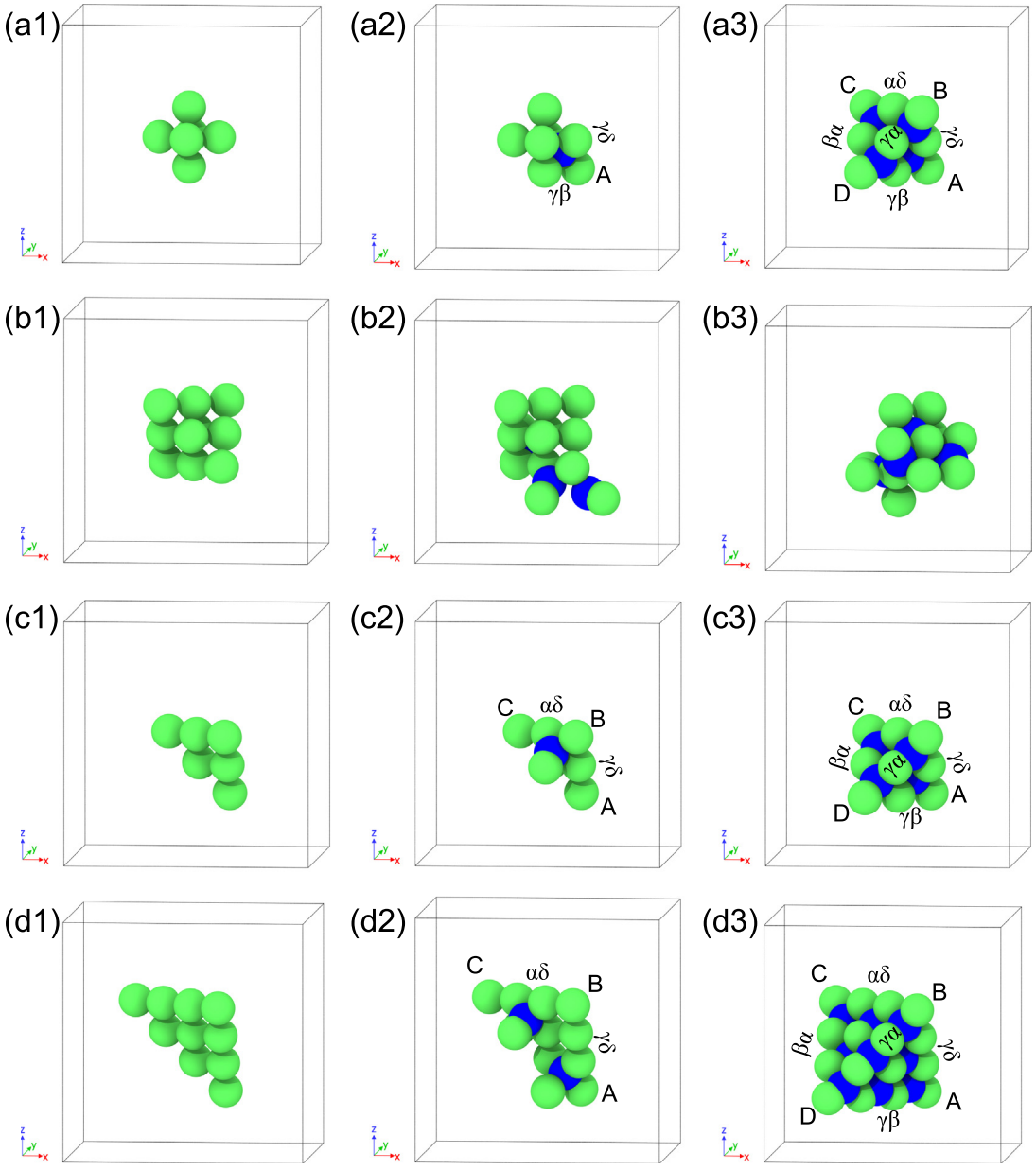

Fig. 3. Transformation of voids and vacancy loops into SFT observed in AIMD: (a1–a3) *v*6-void at 500 K, (b1–b3) *v*10-void at 1000 K, (c1–c3) *v*6-loop at 500 K, and (d1–d3) *v*10-loop at 500 K. For each case, the initial, transformation starting point and final configurations are shown. Vacancies are represented by green spheres while interstitial are represented by blue spheres. (For interpretation of the references to color in this figure legend, the reader is referred to the web version of this article.)

Table 1
The starting time when vacancy loops and voids start to transform to SFT and the completion time when transformation is completed during AIMD simulations (t_i/t_f, in ps). In some cases, perfect SFT are not formed at the end of simulations (2 ps) and only incomplete SFT structures are observed (denoted by NA as not available). The results obtained under 2% volumetric tension strain are also provided.

	Strain free			2% volumetric strain		
	500 K	800 K	1000 K	500 K	800 K	1000 K
3*v*-loop	0.128/0.540	0.096/0.434	0.086/NA	No change	0.140/NA	0.104/NA
6*v*-loop	0.126/0.444	0.096/0.812	0.086/0.884	No change	0.150/NA	0.120/1.506
10*v*-loop	0.182/0.424	0.128/0.452	0.112/0.574	No change	0.368/0.704	0.310/1.216
6*v*-void	0.266/0.398	0.096/0.646	0.082/0.300	No change	No change	0.276/0.478
10*v*-void	No change	No change	0.090/NA	No change	No change	No change

relaxation at $\varepsilon = -2\%$. The results in Fig. 2(b) show that the binding energies of vacancy loops and voids both increase with increasing tensile strain, but those of SFT decrease. In addition, the rate of decrease in binding energies with increasing strain for SFT is rather large, suggesting that the volumetric strain has a significant influence on the stability of SFT in Ni. This effect can be understood by the volume difference associated with SFT, void and loop structures. In general, the volume of the SFT is smaller than that of a vacancy void or loop with the same vacancy number [24]. Therefore, the compressive strain results in unstable vacancy loops, since the creation of loops requires a large volume. On the other hand, the expansion of the lattice makes voids and loops more favorable.

The results obtained at 0 K, as described above, suggest voids are favorable in Ni, which is somewhat inconsistent with experimental evidence. This inconsistency cannot be resolved even by including lattice expansion effects, as in previous works [25]. Therefore, it is expected that the vibrational properties of vacancy clusters play a decisive role in determining their energetics. As it is difficult to study vibrational properties directly for the large supercell used here, the temperature effects are included by performing AIMD simulations at different temperatures from 500 to 1000 K. Owing to computational cost, a $4 \times 4 \times 4$ supercell is used. For selective cases, simulations using a larger $5 \times 5 \times 5$ supercell are also performed to validate the stability of vacancy clusters. A convergence test for energetics is provided in the Supplementary materials. In these dynamical simulations, direct transformations of voids or vacancy loops to SFT are observed. As representative cases, Fig. 3 shows the transformation processes of 6*v* and 10*v* voids and vacancy loops.

The direct transformation of voids to SFT was first proposed by Uberuaga et al. [5] using the parallel replica dynamics based on empirical potentials. Here, the transformation is confirmed by AIMD as evidenced in Fig. 3. For the octahedral 6*v*-void, the surfaces of the void are along {110} planes. The transformation starts with a nearby lattice atom moving towards the center of three vacancies aligned at one plane, creating a local tetrahedron configuration. This reaction creates stair-rod dislocations $\boldsymbol{\gamma\delta}$, $\boldsymbol{\gamma\beta}$ and $\boldsymbol{\beta\delta}$ starting from A, which can be expressed by $\boldsymbol{\gamma A + A\delta = \gamma\delta}$, $\boldsymbol{\gamma A + A\beta = \gamma\beta}$ and $\boldsymbol{\beta A + A\delta = \beta\delta}$. This process continues for the other three planes and finally produces a perfect tetrahedron. The most stable 10*v*-void in Ni is an equilateral tetrahedron, in which all surfaces are {111} planes. This structure is relatively stable and the transformation is only observed at a higher temperature of 1000 K. It is initiated by the movement of a lattice atom towards the triangle edge. The transformation is not completed within 2 ps AIMD runs and only an imperfect stacking fault tetrahedron is produced (Fig. 3(b3)). The whole process is provided as movies in the Supplementary files.

AIMD also reproduces the transformation of vacancy loops to SFT through the Silcox-Hirsch mechanism [27]. As shown in Fig. 3(c) and (d), the neighboring atoms move towards the vacancy loop, which induces the dissociation of loop edge into a stair-rod dislocation and a Shockley partial dislocation *via* reaction type of $\boldsymbol{\alpha B = \alpha\delta + \delta B}$. The following climbing of the Shockley partials leads to the growth of a tetrahedron, with stair-rod dislocations along the edge and intrinsic stacking faults on {111} planes *via* reaction type of $\boldsymbol{\gamma A + A\alpha = \gamma\alpha}$.

Table 1 summarizes the starting time when vacancy loops and voids start to transform to SFT and the completion time when the transformation is completed during AIMD simulations (t_i/t_f). For some cases, the transformation is not completed and only incomplete SFT are observed. The results indicate that the transformation from 6*v*-loop and 10*v*-loop to SFT is very fast (less than 1 ps). The 6*v*-void can also easily transform to a 6*v*-SFT. However, the 10*v*-void is relatively more stable. At a volumetric strain of 2%, the results in Table 1 show that the transformation is delayed compared to strain-free state for both vacancy loops and voids, which support their increased binding energies as shown in Fig. 2.

The AIMD simulations indicate that even if the surface of vacancy clusters is not aligned with the {111} planes, the vacancy clusters can still undergo transformation into SFT. AIMD simulations on some vacancy loops and voids containing non-magical number of vacancies are also performed. The results consistently show transformation processes from vacancy loops and voids to SFT-like defects. A typical example is provided in the supplementary material to illustrate the transformation process of a 13*v*-void to an imperfect 13*v*-SFT. Since only part of SFT-like defects is formed in these simulations, only 6*v* and 10*v* clusters are presented in Fig. 3. These results suggest that SFT are favorable forms of vacancy clusters in Ni at moderate temperatures, consistent with experimental observation [24,28]. These SFT are very stable, and no significant movement is observed after their formation in the AIMD simulations (~2 ps), except for the 3*v*-SFT. This structure is found to be thermodynamically unstable and it can transform back to a vacancy loop even at 500 K. In this transition, an atom in the nearby [111] plane is displaced back and forth towards the vacancy loop. We have calculated the energy barrier for this transition at 0 K, as given in the Supplementary materials. It is found that this transition exhibits a barrier of 0.21 eV, which is way too high, compared to temperatures that we used in AIMD simulations. Especially, this transition is observed even at 500 K. The results indicate that lattice vibrations at finite temperatures tend to change the relative energy between these two structures and decrease the energy barrier, which further makes the transformation observable in MD time scale. Therefore, the thermodynamic stability of vacancy clusters should be interpreted by Gibbs binding free energy consisting of binding energy and binding entropy. However, it is a grand challenge to study the vibrational properties for large vacancy clusters. In this regard, some methods beyond DFT, such as empirical potential approaches, are necessary. Thus the energetics reported here can be used as references to generate such potentials.

In summary, the energetics of different vacancy clusters including SFT, voids, triangular and hexagonal vacancy loops in Ni are studied using first-principles calculations. The binding energy results at 0 K suggest that voids are more stable than SFT. By performing AIMD at finite temperatures from 500 to 1000 K, direct transformations of vacancy loops and voids to SFT are observed. These results highlight the importance of temperature effects in understanding and predicting the stability of vacancy-type defects in *fcc* metals.

Acknowledgement

This work was supported as part of the Energy Dissipation to Defect Evolution (EDDE), an Energy Frontier Research Center funded by the U.S. Department of Energy, Office of Science, Basic Energy Sciences. This research used resources of the National Energy Research Scientific Computing Center, a DOE Office of Science User Facility supported by the Office of Science of the U.S. Department of Energy under Contract No. DE-AC02-05CH11231.

Appendix A. Supplementary materials

The supplementary materials include convergence tests for our calculations, configurations of stable vacancy clusters and supplementary movies which show transformation of 6*v*-voids, 6*v*-loops, 10*v*-voids, 10*v*-loops and 13*v*-void to SFT at different temperatures. In the movies, vacancies are represented by green spheres and interstitials are represented by blue spheres. Supplementary data associated with this article can be found in the online version, at https://doi.org/10.1016/j.scriptamat.2017.10.003.

References

[1] M. Kiritani, Mater. Chem. Phys. 50 (1997) 133–138.
[2] H. Wang, D.S. Xu, R. Yang, P. Veyssière, Acta Mater. 59 (2011) 10–18.
[3] R. Schibli, R. Schäublin, J. Nucl. Mater. 442 (2013) S761–S767.
[4] B.D. Wirth, V. Bulatov, T.D. De La Rubia, J. Nucl. Mater. 283 (2000) 773–777.
[5] B.P. Uberuaga, R.G. Hoagland, A.F. Voter, S.M. Valone, Phys. Rev. Lett. 99 (2007) 135501.
[6] D.S. Aidhy, C. Lu, K. Jin, H. Bei, Y. Zhang, L. Wang, W.J. Weber, Scr. Mater. 114 (2016) 137–141.
[7] K. Nordlund, F. Gao, Appl. Phys. Lett. 74 (1999) 2720–2722.
[8] G. Bonny, N. Castin, D. Terentyev, Model. Simul. Mater. Sci. Eng. 21 (2013) 85004.
[9] G. Bonny, D. Terentyev, R.C. Pasianot, S. Poncé, A. Bakaev, Model. Simul. Mater. Sci. Eng. 19 (2011) 85008.
[10] S. Zhao, G. Velisa, H. Xue, H. Bei, W.J. Weber, Y. Zhang, Acta Mater. 125 (2017) 231–237.
[11] Y.N. Osetsky, A. Serra, M. Victoria, S.I. Golubov, V. Priego, Philos. Mag. A 79 (1999) 2259–2283.
[12] C. Lu, L. Niu, N. Chen, K. Jin, T. Yang, P. Xiu, Y. Zhang, F. Gao, H. Bei, S. Shi, M.-R. He, I.M. Robertson, W.J. Weber, L. Wang, Nat. Commun. 7 (2016) 13564.
[13] K. Kitagawa, K. Yamakawa, H. Fukushima, T. Yoshiie, Y. Hayashi, H. Yoshida, Y. Shimomura, M. Kiritani, J. Nucl. Mater. 133–134 (1985) 395–399.
[14] I.M. Robertson, J.S. Vetrano, M.A. Kirk, M.L. Jenkins, Philos. Mag. A 63 (1991) 299–318.
[15] G. Kresse, J. Furthmüller, Comput. Mater. Sci. 6 (1996) 15–50.
[16] J.P. Perdew, K. Burke, M. Ernzerhof, Phys. Rev. Lett. 77 (1996) 3865.
[17] P.E. Blöchl, Phys. Rev. B 50 (1994) 17953.
[18] S. Zhao, G.M. Stocks, Y. Zhang, Phys. Chem. Chem. Phys. 18 (2016) 24043–24056.
[19] E.H. Megchiche, C. Mijoule, M. Amarouche, J. Phys. Condens. Matter 22 (2010) 485502.
[20] S. Plimpton, J. Comput. Phys. 117 (1995) 1–19.
[21] G.P. Purja Pun, V. Yamakov, Y. Mishin, Model. Simul. Mater. Sci. Eng. 23 (2015) 65006.
[22] Q. Peng, X. Zhang, G. Lu, Model. Simul. Mater. Sci. Eng. 18 (2010) 55009.
[23] N.Q. Lam, L. Dagens, J. Phys. F Met. Phys. 16 (1986) 1373–1384.
[24] R.J. Olsen, K. Jin, C. Lu, L.K. Beland, L. Wang, H. Bei, E.D. Specht, B.C. Larson, J. Nucl. Mater. 469 (2016) 153–161.
[25] E.H. Megchiche, S. Pérusin, J.-C. Barthelat, C. Mijoule, Phys. Rev. B 74 (2006) 64111.
[26] X. Lu, M. Selleby, B. Sundman, Calphad 29 (2005) 68–89.
[27] J. Silcox, P.B. Hirsch, Philos. Mag. 4 (1959) 72–89.
[28] Y. Zhang, K. Jin, H. Xue, C. Lu, R.J. Olsen, L.K. Beland, M.W. Ullah, S. Zhao, H. Bei, D.S. Aidhy, G.D. Samolyuk, L. Wang, M. Caro, A. Caro, G.M. Stocks, B.C. Larson, I.M. Robertson, A.A. Correa, W.J. Weber, J. Mater. Res. 31 (2016) 2363–2375.